https://doi.org/10.15407/ufm.26.01.124

M.O. VASYLYEV [1,*], B.M. MORDYUK [1,], S.M. VOLOSHKO [2,***], and P.O. GURIN [3,****]**

[1] G.V. Kurdyumov Institute for Metal Physics of the N.A.S. of Ukraine, 36, Academician Vernadsky Blvd., UA-03142, Kyiv, Ukraine

[2] National Technical University of Ukraine 'Igor Sikorsky Kyiv Polytechnic Institute', 37 Prospect Beresteiskyi, UA-03056 Kyiv, Ukraine

[3] P.L. Shupyk National Healthcare University of Ukraine, 9, Dorogozhytska Str., UA-04112 Kyiv, Ukraine

* vasil@imp.kiev.ua, vasil1934@ukr.net, ** mordyuk@imp.kiev.ua, *** voloshkosvetlana13@gmail.com, **** dr.huryn17@gmail.com

PHYSIOLOGICAL CORROSION AND ION RELEASE IN DENTAL Co–Cr–Mo ALLOYS FABRICATED USING ADDITIVE MANUFACTURING

The aim of the article is to review the aspects of the corrosion behaviour, which are most relevant to the clinical application of dental metal alloys. From the point of view of biocompatibility, two corrosion phenomena are considered: the degradation of the surface of dental products and the ion release of alloying atoms during exposure to an artificial physiological environment. While corrosion leads to the partial loss of the material strength, the ion release phenomenon causes cytotoxicity, allergy, and other biological influences in the human body. As noted, the Co–Cr-system alloys are widely known for their biomedical applications in the orthopaedic and dental fields due to their low cost and adequate physical-mechanical properties. The review analyses the microstructure and electrochemical properties of the commercial dental Co–Cr–(Mo, W) alloys fabricated by traditional casting techniques and additive manufacturing by means of the selective laser melting (SLM). Currently, SLM is the most promising technique among the emerging additive fabrication technologies used for metal-products' manufacturing in dentistry.

Keywords: additive manufacturing, dental alloys, microstructure, dentistry, corrosion, ion release.

Citation: M.O. Vasylyev, B.M. Mordyuk, S.M. Voloshko, and P.O. Gurin, Physiological Corrosion and Ion Release in Dental Co–Cr–Mo Alloys Fabricated Using Additive Manufacturing, *Progress in Physics of Metals*, **26**, No. 1: 120–145 (2025)

1. Introduction

One of the most fundamental requirements to any biomaterial implanted in the human body is that it should be biocompatible and not cause undesirable adverse effects because it directly reacts with the surrounding body tissues or fluids [1–4]. In particular, biomaterials based on metals or metal alloys can be used in objects such as implants, plates, screws or surgical instruments as the replacement for human body parts. These materials should meet the requirements not only for biocompatibility but also for the good mechanical strength and corrosion resistance. It is known that the corrosion resistance is the effective prognostic of the biocompatibility and further application of these metallic materials [5]. Over time, the metal alloy itself and its corrosion products can be transported by the bloodstream to distant organs or be partially eliminated by body fluids. The internal organs such as the liver and kidney can accumulate the metal corrosion products; the tolerance level may be exceeded, leading to conditions under which certain diseases may be provoked [6].

Metallic biomaterials for temporary and long-term use are applied in the different branches of medicine including the dental sphere [7–9]. The biological effects of the material released into the tissue are the subject of much concern and investigation of the ability of the metallic implants upon degradation to stimulate metal sensitivity reactions in humans and animals. It is apparent that many patients have sensitivity to the metals and they will elicit inflammatory responses and sometimes the formation of the foreign body giant cells. This may have an adverse effect on the performance of the implant, *i.e.*, the pain, swelling, and tissue necrosis at the site and, in some cases, loosening of the implant. Studies on implant site infections revealed that infection rates are altered by the presence of this tissue response.

Particularly, it is well known that in living organisms the saliva and other external factors create an extremely aggressive biomechanical environment in the human oral cavity. Concerning dental applications, the oral environment and saliva are composed of organic and inorganic aggressive components. Thus, the corrosion resistance and chemical stability of dental alloys are essential for clinical success [10–12]. Several factors, such as oxygen, changes in the pH levels, temperature, and aggressive anions, contribute to the corrosion in the oral environment. On the other side, the resistance of the metal alloy to corrosion in the oral cavity is a very important factor in the choice of restorative non-precious dental alloys. It is known in clinical practice that insufficient corrosion resistance leads to unacceptable colouring, porosity and weakening of mechanical properties of dental materials.

The alloys of the Co–Cr–Mo systems have been widely used in dental and orthopaedic implant applications due to its excellent mechanical pro-

perties (high hardness and ultimate strength), wear and corrosion resistance, as well as a good biocompatibility [13–20]. Even though many high-strength ceramic systems, such as stabilized zirconia, alumina and lithium disilicate ceramics are available in clinical dentistry, due to their favourable characteristics and acceptable price, the Co–Cr system alloys play nowadays the predominant role amongst metals used in dentistry. Cast CoCr alloys mainly exhibit the mixture of γ (f.c.c.) and ε (h.c.p.) phases. It has also been observed in many heat-treatment experiments that the carbides of a $M_{23}C_6$-type (where M is a metal) precipitate along the grain boundaries. Heat treatment eliminates the crystal defects, such as dislocations, and stabilizes the microstructure, which leads to the reduction of the residual stress. In this respect, the temperature of the solution heat treatment is the most important factor, affecting the hardness, strength, and ductility of the alloy. This affects its fracture strength, fatigue life and wear resistance. It may also affect the corrosion resistance.

The Co–Cr–Mo-based alloys have been used in dentistry since 1929, mainly for frameworks in removable partial dentures. In the last decades, application to the manufacture of fixed partial dentures is increasing. The extensive use of these alloys relies on their superior resistance to corrosion and biodegradation and on their good mechanical properties, including high ultimate tensile and fatigue strength combined with sufficient elongation at fracture and high biocompatibility. In these alloys, the chromium oxide film is spontaneously formed which protects the metal from the surrounding environment, controls the corrosion behaviour of the material, the interaction with tissues and body fluids and therefore is responsible for the material high biocompatibility [6]. The relatively high corrosion resistance of Co–Cr-based alloys is attributed to the formation of the passivating protective metal oxide film [21, 22]. It is generally accepted that the composition of this film is predominantly Cr_2O_3 oxide with some minor contribution of other oxides (Co- and Mo-oxides, especially if the film is air formed) and the $Co(OH)_3$ species [23, 24]. The physicochemical properties of such passive film control the material's corrosion behaviour, the interaction with tissues and the surrounding part replaced into the body and thus the grade of the material's biocompatibility. Although the thickness of these passive films is typically only a few nanometres, they act as the highly protective barrier between the metal surface and the aggressive biological environment. The rate of ion transfer determines the protectiveness of the passive film through the film, as well as the stability of the film against dissolution (Fig. 1). A variety of factors can influence ion transport through the film, such as the films' chemical composition, structure, thickness and presence of defects. Principally, the nature and of the passive film stability on the particular metal or alloy depends on the environmental conditions, such as the composition of the electrolyte, the redox conditions, the exposure time and temperature.

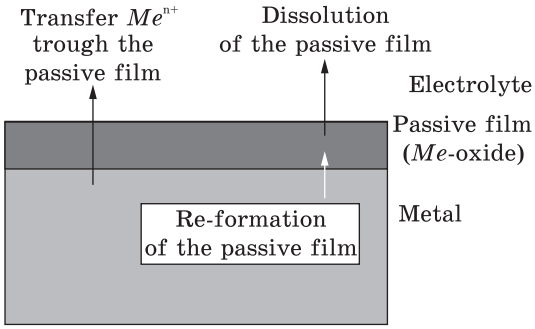

Fig. 1. Schematic illustration of a passive surface [21]

The corrosion resistance of these biomaterials is affected by several factors, such as the alloy itself (*e.g.*, chemical composition, microstructure and surface state), the characteristics of the environment (pH, temperature), and the manufacturing techniques involved [25, 26]. For the metal materials to be implanted in the human body, corrosion is the first consideration because the release of metal ion occurs mainly due to the chemical reactions of the dental restorations [27]. Metal is sensitive not only to small metal ions but also to the complex of the metal ions and host tissue. The nature of the metal ion binding to tissue or cells, the distribution of the metal ion or metal complexes in the body, and the biological responses to these complexes are of concern. Co and Cr metal ions effuse from joint materials and migrate into surrounding tissue during long-time use, giving rise to further negative effect on the biocompatibility, the mechanical integrity, and serious clinical problems (such as failure of the embedded joint, local osteolysis, local toxicity, systemic toxicity, and allergic reactions) [28–31].

Since the metal release from implants is an important subject, numerous studies, including long-term clinical studies, have been conducted on metal release from the dental restorations into body fluids (serum, urine, *etc.*). The mechanism of metal ion release from metallic implant materials and the behaviour of released metal ions *in vivo* are discussed according to empirical data. It occurs by various mechanisms, including (a) uniform passive dissolution resulting from the slow diffusion of the metal ions through the passive film; and (b) the local breakdown of the passivity as the consequence of the various types of localized corrosion, or various mechanical events such the fretting corrosion [32–35].

To produce the CoCr-based alloy dental restorations the lost-wax casting and hot forging processes are usually used. However, the components with the complex shape produced by the casting process have their strength is not high enough. Besides this consuming process has many steps and technological errors [36] Also, the cast alloys having inhomogeneous microstructure, solidification defects, segregation and large grains are not sufficient to ensure high quality, superior physical and chemical properties leading to a long service life [37].

To solve the indicated problems with the traditional casting processes, currently additive manufacturing (AM) is being accepted as the novel candidate for the fabrication of the customized dental restorations. Current-

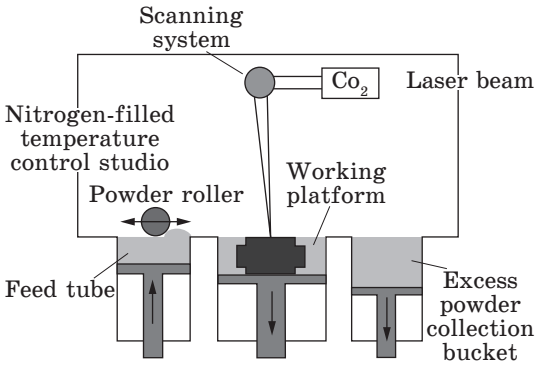

Fig. 2. The SLM process [49]

ly, AM is becoming increasingly popular for a variety of applications, particularly in the fields of the aerospace, energy, and automotive industries. This method is in contrast to traditional subtractive manufacturing (milling, welding, casting, forming, forging and turning) which is based on the mechanical removal of the unneeded material part to form the desired component with complex geometries. Among the advantages of AM, there is producing without additional equipment, including tools, gauges or fixtures, this tool-free production approach can provide flexibility in design, personal customization, high precision in complex parts, reduced energy and material use, and shortened time for implementation. In addition, manufacturing components have no geometric limitations [38, 39]. Metal AM technology is a process of joining materials layer by layer to produce parts based on the predesigned three-dimensional model data, which is distinguished from traditional subtractive machining techniques. A large number of publications have shown that AM procedure provides the efficient and fast technique to digitally design and manufacture biocompatible metal frameworks for complex dental prostheses with improved physical and chemical properties, such as strength, durability and corrosion resistance with not-so-high metal release [40–43].

The following most important AMs can be distinguished for metal printing, namely, selective laser melting (SLM), selective laser sintering (SLS), and electron beam melting (EBM). Recently, among the different additive methods SLM has attracted the worldwide interest of research groups as very promising technique for the manufacturing of the dental metallic structures, such as dental implants, crowns, bridges and prosthetic groups with complex geometry [44–48]. In prosthetic dentistry, most studies on SLM have focused on the dental alloys of a Co–Cr–Mo system used to manufacture prosthetic dentistry. Studies have also shown that prostheses fabricated with SLM have better corrosion resistance and higher strength in comparison with those fabricated with conventional casting methods.

SLM is the AM procedure that allows the direct printing of the metal component using the three-dimensional computer-aided design (CAD) by fusing fine metal powder in the layers by the high-power laser beam quickly and precisely (Fig. 2). SLM printers use CO_2 lasers or fibre lasers (Nd:YAG or Yb:YAG) [49, 50]. The laser beam is focused on the powder, and the energy supplied by the laser can melt it. The melting process can

be adjusted by varying the wavelength, laser source and power. Metal powders intended to be used in the printing process should be spherical and have a stringent particle size distribution to achieve good packing behaviour. The powders for the next layer are covered on the melted layer, and the laser is again scanned according to the next sliced data providing the layer-by-layer manufacturing on the base plate. This sequence continues until the near-net-shape products are formed automatically. SLM can fully melt the metal powder into three-dimensional solid printed parts. The main controllers in SLM are the process parameters, which include, for example, laser power, scan speed, hatch spacing, and scan strategy, which will consequently produce specific microstructure and part properties.

The main goal of this review is to compare the physiological corrosion and ion release effects in the Co–Cr–Mo alloy samples manufactured by two technologies, *i.e.*, conventional casting and SLM, which are usually used in the metal dentistry. This review attempts to include the related latest research in the chronological order.

2. Corrosion in the Simulated Physiological Solution

The microstructure, surface properties, hardness, and corrosion behaviour of the Co–Cr–Mo alloy samples fabricated by the SLM technique and compared with those of the casting one were investigated previously in Ref. [51]. The SLM samples were manufactured using Germany BEGO Medical Fibre Laser with such parameters: power is of 200 W; jogging speed is of 20.7 m/s; spot size is of 50 μm; layer thickness is of 20–100 μm. The Co–Cr–Mo alloy powder, containing (wt.%) Co 61.5, Cr 26.0, W 5.0, Mo 6.0, Si, and Fe, was used in this study. The flame-casting samples had the same content. The surface of both types of samples was etched for 30 s with hydrochloric acid/hydrogen peroxide at room temperature. The corrosion tests were performed on quintuplicate cylindrical samples in the artificial saliva solution: 0.1 g/L sodium chloride; 1.3 g/L potassium chloride; 0.1 g/L calcium chloride dehydrate; 0.05 g/L magnesium chloride hexahydrate; 0.5 g/L polypeptone; 0.000025 g/L sodium fluoride; 0.027 g/L potassium dihydrogen phosphate; and 0.035 g/L potassium dihydrogen phosphate with pH = 7.0, at 37 ± 0.5°C. Every sample was accessed to reach an open circuit potential (E_{corr}) for 30 min. E_{corr} was recorded and then the potentiodynamic test was started within the scanning range from −250 to +1.600 mV (*vs.* the reference electrode) at the sweep rate of 1 $mV \cdot s^{-1}$. The obtained data were analysed using the curve-fitting mode of the specialized Power Suite software to calculate the corrosion current (I_{corr}) and the polarization resistance (R_p) of the alloy samples [52].

Secondary electron images of the SLM and the cast samples are shown in Fig. 3. The cast samples (Fig. 3, *a*) show one solid solution matrix of the crystalline phase with the typical dendritic morphology. In contrast,

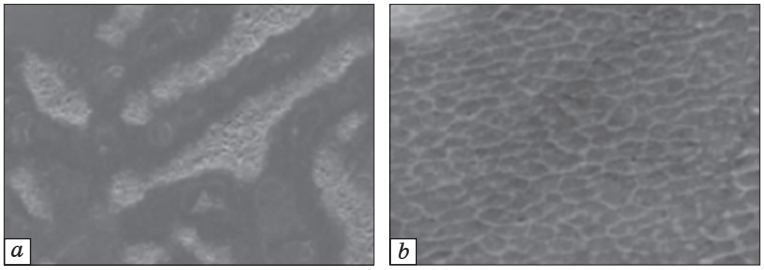

Fig. 3. Secondary scanning electron microscopy images: SLM (*a*) (magnification $\times 10^3$) and cast (*b*) (magnification $\times 10^4$) samples [51]

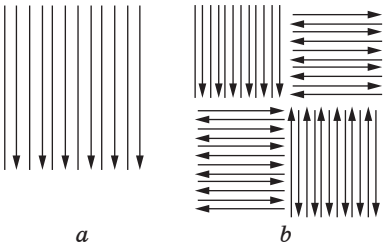

Fig. 4. The illustration of the line scanning strategy (*a*) and island scanning strategy (*b*) [53]

the SLM samples (Fig. 3, *b*) demonstrate the dendrite-like structural morphology (at ×10 000 magnification) and show the cellular structure with each cell size of about 1 μm. This might indicate that these parts belonged to one solid solution, and the SLM samples had homogeneous microstructure. The grain size of the SLM samples is much smaller than that of the cast samples.

The corrosion current (I_{corr}) and the polarization resistance (R_p) of the SLM and cast samples, as results of the potentiodynamic tests are shown in Table 1. In this study, the potentiodynamic tests exhibited practically no statistically significant differences between the two samples. They demonstrated good anti-corrosion behaviour in the saliva solution. It was thus indicated that the SLM-printed parts could also meet the needs of the dental clinics.

In Ref. [53], Co–Cr–W alloy samples were fabricated by SLM using line and island-scanning strategies to identify the corrosion parameters that can obtain expected Co–Cr–W parts for dental applications. The commercial Co–Cr–W alloy powders containing (wt.%) Co 60.5, Cr 28.0, W 9.0, Si 1.5, Mn < 1.0, and Fe < 1.0 were used in this study. The samples were fabricated by the SLM technique (Mlab-R, CONCEPTLAER, Germany) using two varieties of laser scanning strategies: line scanning and island

Table 1. **Corrosion current (I_{corr}) and polarization resistance (R_p) of the SLM and cast samples [51]**

Sample type	I_{corr}, μA/cm^2	E_{corr}, V	R_p, kΩ cm^2
SLM	0.02	–0.32	977.383
Cast	0.07	–0.39	1129.9

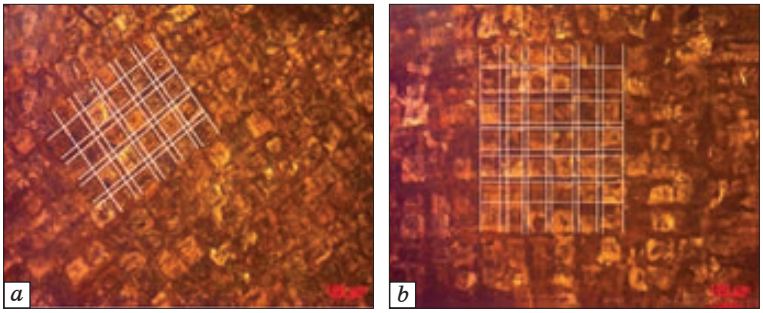

Fig. 5. The optical metallographic structure: (*a*) the polished line-formed sample; (*b*) the polished island-formed alloy. Magnification is ×100 [53]

scanning strategy, as illustrated in Fig. 4, *a*, *b*. For SLM printing, the next processing parameters were used for both scan strategies: laser power 95 W; scan sped 700 mm/s; powder thickness 25 μm; island 2×2 mm (island strategy).

To evaluate the corrosion resistance in the standard phosphate-buffered saline (PBS) at 37 °C, the electrochemical test was conducted using the three-electrode cell. The platinum was the counter electrode and the saturated calomel electrode was the reference electrode. The sample with an exposed area of 1 cm^2 was the working electrode. The polarization scan was started from the anodic region from 250 mV below open circuit potential at a constant voltage scan rate of 0.5 mV/s. Before performing this study, the samples were ground with waterproof emery paper to 1200 grit under running water, then ultrasonically cleaned in acetone for 15 min, rinsed in distilled water and finally dried at room temperature.

The XRD patterns of the line formed and island strategy demonstrated that both samples exhibit γ (f.c.c.) and ε (h.c.p.) phases. Interestingly, the island-strategy-formed sample exhibits a much higher diffraction intensity of the e phase compared with the line-formed sample. Figure 5 shows the optical micrograph of the top view of both samples. As seen, the micrographs exhibit a distinctive square-like pattern with the surrounding border as denoted by white lines in Fig. 5, *a, b*. The edge length of the square is 60±5 μm, whilst the width of the border is 20±3 μm and the border presents to be darker whereas the square-like structure (central zone) is brighter. In addition, the square-like patterns of the line-formed samples appear to be more uniform compared with the island-formed specimens. It is noteworthy from the XRD patterns that the peak intensity of island-formed sample from the ε-phase is greater than that of the line-formed sample. This fact is explained by the more un-melted powder on the island-formed sample surface.

Polarization parameters, including corrosion potential (E_{corr}), corrosion current density (I_{corr}), polarization resistance (R_p), and corrosion rate

in PBS solutions were obtained from the polarization curves listed in Table 2. The anodic branches of the polarization curves for both samples in PBS solutions exhibit a similar passive region at a similar potential range, which is at the potential of 0 to 0.5 V. As can be seen in Table 2, the line-formed samples show slightly higher corrosion potential (E_{corr}) but the slightly lower corrosion current density (I_{corr}). This fact indicates that the corrosion resistance of the island-formed samples is slightly greater than that of the line-formed samples. In addition, this is further demonstrated by the higher values of the polarization resistance R_p and lower corrosion rate of the island-formed alloy as compared to the line-formed samples in the simulated body solutions.

In Ref. [54], the SLM technique was used to produce two different types of Co–Cr–Mo alloy samples investigated in the solutions simulating biological fluids. The selected SLM parameters allow obtaining samples with different microstructural characteristics: the *B*2 sample has a higher porosity than *B*1, but a finer cellular microstructure. The commercial Co–Cr–Mo alloy powders were used in this study. They contained (wt.%) Cr 27–30, Mo 5–7, Mn < 1.0, Fe < 0.75, Ni < 0.5, W < 0.2, and C < 0.04, and balanced by Co. The samples were fabricated using two different sets of parameters, as indicated in Table 3.

All samples were exposed to the solutions that simulated body fluids (SBF) for 15 days at a temperature of 37 ± 1 °C. To monitor the evolution of the corrosion behaviour during the immersion period electrochemical impedance spectroscopy (EIS) was used (Table 4).

Table 2. **The polarization parameters obtained from the polarization curves [53]**

Sample type	I_{corr}, nA	E_{corr}, mV	R_p, Ω	Corrosion rate, 10^{-4} mm/year
Line–PBS	20.20	–201	1.790	4.60
Island–PBS	19.70	–200	1.855	4.50

Table 3. **Process parameters used and obtained relative densities [54]**

Test	Power, W	Scan speed, mm/s	Fluence, J/mm³	Relative density, %
*B*1	150	900	138.8	99.8
*B*2	90	1200	53.6	95

Table 4. **Composition, electrical conductivity and pH of simulated body fluid (SBF) solution [54]**

Na_2HPO_4, g/L	KH_2PO_4, g/L	KCl, g/L	NaCl, g/L	Total Cl^{-1}, M	Λ, μS/cm	pH
1.42	0.245	0.2	8.8	0.15	17.15	7.4

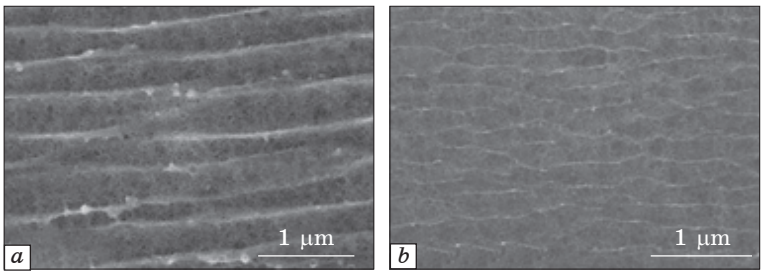

Fig. 6. SEM image of the microstructures of (*a*) *B*1 and (*b*) *B*2 samples after electrolytic etching [54]

The used laser parameters (Table 3) give rise to the different morphological of the microstructure in the fabricated samples. High fluence processes promoted powder melting instead of sintering, enabling the production of denser samples. In particular, sample *B*1 fabricated under high laser conditions showed the high relative density (99.85%) and a low level of residual porosity. However, the *B*2 samples obtained with a low fluence process are characterized by the lower relative density (95%) with some large pores (up to 200 μm). The examples of the observed microstructure are shown in Fig. 6. For both types of samples, the SEM show the fine and elongated cellular microstructure formed within the melt pool. The high solidification rates and a high level of non-equilibrium conditions during SLM induced the development of the microcellular structure and suppressed the formation of the microsize carbides. The difference in the microcells size in the two samples is observed: the sample *B*1 (Fig. 6, *a*) is characterized by the coarser microcells concerning the sample *B*2 (Fig. 6, *b*). It is because to the higher laser scanning speed and the lower laser fluence for the sample *B*2, which promoted the cell size refinement, due to a shorter persistence at the high temperature during the layers printing.

According to x-ray diffraction data in all samples, the metastable γ (f.c.c.) phase is mainly presented at room temperature. In addition, some amount of ε (h.c.p.) phase was detected on both SLM samples. This is owing to the $\gamma \rightarrow \varepsilon$ phase transformation partially occurred during each new layer printing up. The x-ray diffraction data indicated a higher amount of the e phase in the *B*2 samples with respect to the *B*1 one.

The corrosion behaviour of the SLM alloy samples was studied by monitoring the E_{corr} and I_{corr} data of both sample types, during 15 days of exposure to the selected SBF (Fig. 7, *a*, *b*). At short immersion time, both *B*1 and *B*2 showed passive behaviour and low corrosion currents (I_{corr}) around $9 \cdot 10^{-8}$ and 10^{-7} A/cm^2 for *B*1 and *B*2 samples, respectively. But, after 15 days of immersion time, the anodic currents significantly decreased, particularly for the *B*2 sample, inducing the ennobling of E_{corr} and the reduction of I_{corr} down to $2 \cdot 10^{-8}$ A/cm^2 for the *B*1 sample and $9 \cdot 10^{-9}$ A/cm^2 for the *B*2 sample. Such results confirmed the process parameters affect the corrosion behaviour: sample *B*2 has lower corrosion rates than sample *B*1 in all tested conditions. In conclusion, it can be

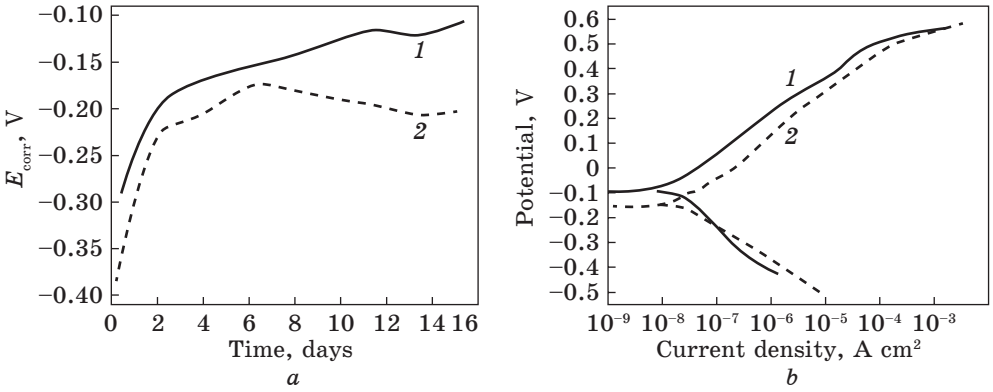

Fig. 7. The corrosion behaviour of the *B*1 and *B*2 samples during the exposure to SBF: *a* — dependence E_{corr} on the exposure time values; *b* — polarization curves recorded; *1* and *2* — *B*1 and *B*2 samples, respectively [54]

noted that both types of samples showed low corrosion rates due to the formation of the very protective oxide film on the sample surfaces with high resistance to localized corrosion, and the finer microstructure ensured slightly higher corrosion resistance.

The aim of the study [12] was to investigate the corrosion properties of Co–Cr alloy samples manufactured by different technologies, namely by SLM (as-printed and further heat-treated) and conventionally cast alloy with identical chemical compositions.

Three different Co–Cr alloy samples were examined, each having the same chemical composition, containing 59% Co, 27% Cr, 9.5% W, 3.5% Mo, 1% Si, and less than 1% of C, Fe, Mn, and N. The first sample type was manufactured using SLM (denoted as SLM), while the second type was additionally studied after heat treatment at 1050°C and furnace cooled (denoted as SLM-HT). For SLM printing, the next parameters were used: laser power was set at 70 W; laser travel velocity of 520 mm/s; hatch distance of 25 μm; the layer thickness of 25 μm and the calculated energy density was 215.4 J/mm^3. The casted samples are denoted as REF. All samples were ground and polished until a mirrored surface was achieved, and then electrolytically etched in 100 ml H_2O + 4 ml HCl, by applying the voltage of 5 V for 6 s, to reveal the microstructure.

Corrosion properties were evaluated by short and long-term electrochemical tests and 42 day in artificial saliva, artificial saliva containing fluoride and acidified artificial saliva at 37 °C. Electrochemical tests were performed using the potentiostat in the sequence containing non-destructive measurements: open circuit potential measurement for 6200 s, and linear polarization in the range ±20 mV (*vs.* E_{corr}) at a scan rate of 0.1 mV/s. A three-electrode corrosion cell was used, with the working electrode embedded in a Teflon holder. The Ag/AgCl electrode served as the reference

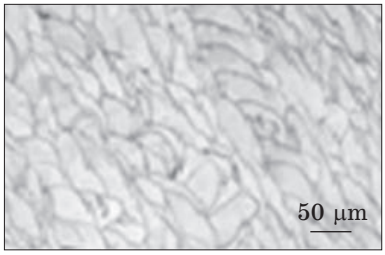

Fig. 8. Microstructural SEM image of the samples produced by SLM [12]

electrode and glassy carbon was used for the counter one. The solution for tests was artificial saliva (AS) with the chemical composition as follows: 0.6 g/L NaCl, 0.72 g/L KCl, 0.22 g/L $CaCl_2 \times 2$ H_2O, 0.68 g/L KH_2PO_4, 0.856 g/L $Na_2HPO_4 \times 12$ H_2O, 0.060 g/L KSCN, 1.5 g/L $KHCO_3$ and 0.03 g/L citric acid with the pH of this solution 6.5. The electrochemical tests were also conducted in saliva containing 1450 μg/mL of fluoride ions, through the addition of 3.15 g/L NaF (AS + NaF), and acidified saliva (AS + lactic acid), containing 0.1 mole/L of lactic acid, with a pH of 2.3 ± 0.1.

Microstructural examination of the casted samples (REF) showed the dendritic morphology. Microstructural images of the Co–Cr samples produced by SLM printing display the formation of the typical columnar structure with overlapping regions of the melting pools (Fig. 8). In this case the dominating γ-phase is present with a small quantity of the ε-martensitic phase. In the heat-treated SLM-produced samples, the microstructure displays less pronounced features associated with the previous (SLM) grown structures. The reduced texture effect occurs due to the precipitation of additional phases and redistribution of the alloying elements. As such, the original melt pool structures and the columnar structure dissolve and reform, leaving an arrangement pattern of various precipitates. The fine needle-like precipitation, enriched with Cr (approximately 30 at.%), develops across the material, evenly forming within γ-phase.

Electrochemical parameters deduced from the potentiodynamic curves for the REF, SLM and SLM-HT samples exposed in AS, AS + NaF and AS + lactic acid at 37 °C are presented in Table 5. For all three immersion environments studied, the measured potential increased in all samples.

Table 5. **Electrochemical parameters [12]**

Solution	Sample type	E_{corr}, V	I_{corr}, μA/cm^2
AS	REF	−0.532	0.0155
	SLM	−0.28	0.0539
	SLM-HT	−0.176	0.0278
AS + NaF	REF	−0.303	0.032
	SLM	−0.348	0.0352
	SLM-HT	−0.243	0.0836
AS + lactic acid	REF	−0.20	0.0102
	SLM	−0.2	0.0264
	SLM-HT	−0.260	0.0244

3. Metal Ion Release in the Simulated Physiological Solution

In vitro biocompatibility of Co–Cr–Mo–W alloy samples fabricated by SLM and traditional casting techniques were tested in the artificial saliva solution [58]. Eleven cylindrically shaped specimens (10 mm diameter and 3 mm thickness) were prepared by a flame-cast method (traditional casting group) from a Co–Cr–Mo–W alloy with a composition (wt.%) of Co 63.9, Cr 24.7, W 5.4, Mo 5.0, and trace amounts of Si. All samples were ground wet with a series of silicon carbide (SiC) papers (400, 800, and 1200 grit) using a grinder-polisher machine (Beta, Buehler, Lake Bluff, IL, USA). Before use, samples were ultrasonically cleaned in ethanol and deionized water for 5 min. Immersion tests incubated three samples from each group in the artificial saliva solution (0.1 g/L NaCl, 1.3 g/L KCl, 0.1 g/L $CaCl_2$ $2H_2O$, 0.05 g/L $MgCl_2$ $6H_2O$, 0.5 g/L polypeptone, 0.000025 g/L NaF, 0.027 g/L KH_2PO_4, and 0.035 g/L K_2HPO_4; pH¼7.0). Each sample was cultivated in a closed sterile centrifuge tube containing 7.5 ml of the artificial saliva solution at 37 °C for 7 days. After 7 days, samples were removed and the solutions were tested for metal ion release by inductively coupled plasma atomic emission spectrometry (ICP-AES Vista AX; Varian, Palo Alto, CA, USA), using matrix-matched standards.

Figure 9 shows the microstructure of the traditional cast and SLM samples. At a magnification of ×100, cast specimens (Fig. 9, *a*) exhibited the typical dendritic solidification microstructure consisting of the dendrites (light portion Fig. 9, *a*), the interdendritic region (dark portion) and the third part manifesting as dark lines in the light portion. In contrast, the SLM samples (Fig. 9, *b*) exhibited a homogeneous and compact structure.

Table 6 shows the quantity of the metal ions released in the artificial saliva solution over 7 days from either traditional-cast or SLM samples. The releases of Co and Mo were significantly different between the two groups, with the SLM group showing lower levels of Co and Mo ions than the traditional-cast samples. As the cast group was observed to have a heterogeneous structure and the SLM consisted of a homogeneous and compact structure (Fig. 9), this microstructural difference may account for different Co ion release characteristics in the two sample types.

The study [56] aims to elucidate the difference in the metal release effect for Co–Cr–Mo alloy samples fabricated by SLM using three different sets of laser scanning parameters, compared with the cast alloy samp-

Table 6. **Metal-ion release in the artificial saliva solution (mg/cm^2). Here, 'dl' indicates 'detection limit' [55]**

Sample type	Co	Cr	Mo
CAST	0.49 (0.13)	dl	0.12 (0.015)
SLM	0.12 (0.04)	dl	0.015 (0.007)

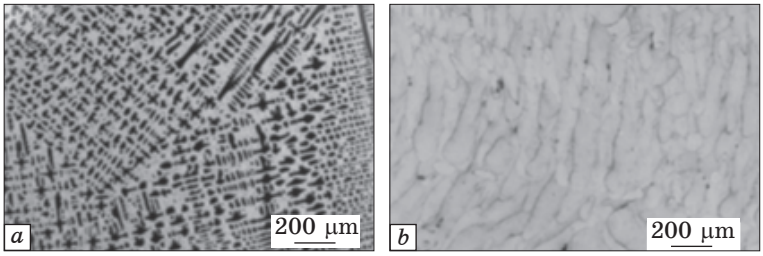

Fig. 9. Metallographic images of the cast samples (*a*) and the SLM sample (*b*) [55]

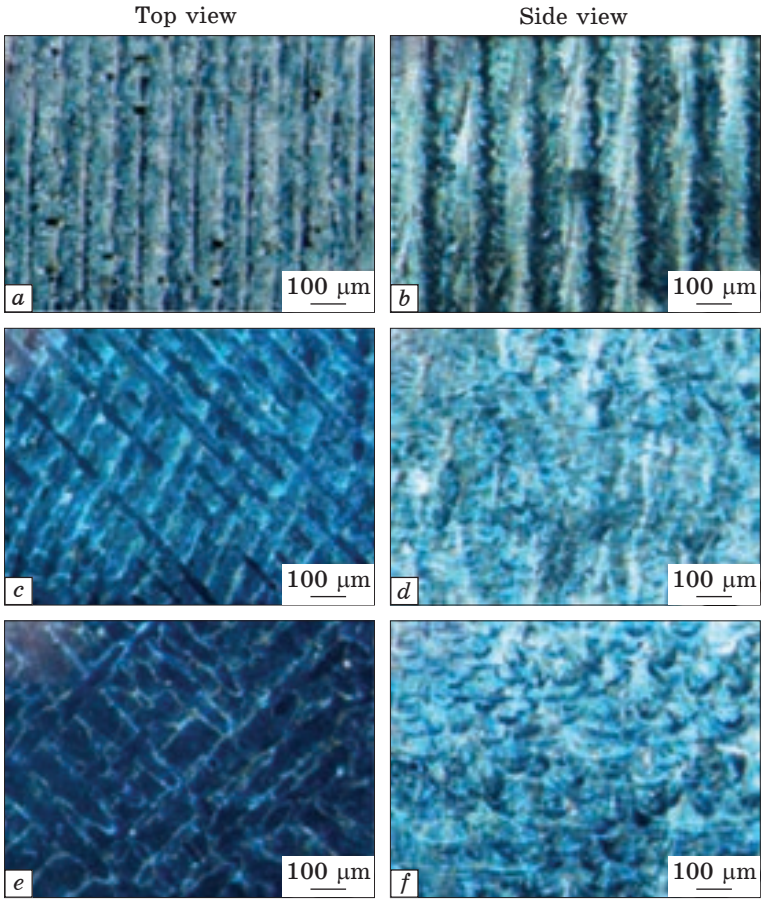

Fig. 10. Optical microscopy (OM) images (×100) of SLM samples fabricated by different scanning strategies: L20 (*a, b*), R20 (*c, d*), and R40 (*e, f*). Here, *a, c*, and *e* demonstrate the top-view images; *b, d*, and *f* demonstrate the side-view (cross-sectional) images [56]

les. The detailed SLM process parameters are given in Table 7. The Co–Cr alloy powder containing (wt.%) Co 60–65, Cr 26–30, Mo 5–7, Si < 1, Mn < 1.0, and Fe < 0.75, C < 0.16 and Ni < 0.1–0.2 was used in this study. The powder size was 25 μm (5–40 μm). Released amounts of the individu-

al metals (Co, Cr, and Mo) per surface area from the SLM and cast samples were determined after exposure to the phosphate-buffered saline (pH 7.3±0.1) during 2 and 168 h. Before exposure, the samples were ground using 1200 grit SiC, ultrasonically cleaned in acetone and isopropyl alcohol for 7 min, respectively, dried with cold nitrogen gas, and aged (desiccator, room temperature) for 24±1 h to achieve a defined and stable surface oxide. The samples were completely immersed in the vertical position (a surface area to solution volume ratio of 1 $cm^2 \cdot mL^{-1}$) in PBS. The chemical composition of PBS was 8.77 g/L NaCl, 1.28 g/L Na_2HPO_4, 1.36 g/L KH_2PO_4, 370 µL/L 50% NaOH and ultrapure water (18.2 M W cm) [57]. Solution metal analysis (total metal) was performed using atomic absorption spectroscopy (AAnalyst 800, Perkin Elmer) with flame (for Co) and graphite furnace (for Co, Cr and Mo) modes.

As one can see from optical microscopy (Fig. 10), regardless of the fabrication parameters the laser-melted microstructure was strongly heterogeneous. On the macro-level, the accumulative rapid solidification of the adjacent melt pools revealed the network appearance of the stacked melt pools as illustrated in the top-view and of half-cylinders (melt pool boundaries) shown in the side-view images (cross-sections) in Fig. 10. The microstructure of all three etched SLM samples shows of the fine cellular (≈1 µm) and elongated cellular the microstructural features.

Table 8 demonstrates the metal ion released proportion of the main alloy constituents, is not proportional to the bulk composition. In particular, Co ions are preferentially released from all samples (>95 wt.%), independent of the manufacturing parameters, solution and exposure period. Most metal ions (Co + Cr + Mo) are released during the first 2 h of the exposure, with less than a 4.4-fold increased amount up to 168 h. This corresponds to the more than 38-fold lower metal release rate after 168 h

Table 7. **SLM parameters [56]**

Sample type	Angle, deg	Laser power, W	Laser scan speed, mm/s	Scan spacing, mm	Powder stacking thickness, µm
R40	60	195	535	0.14	40
R20	60	195	800	0.1	20
L20	0	195	800	0.1	20

Table 8. **Released amounts of Co, Cr, Mo [56]**

Element	Cast (RBS 2 h), µg/cm²	SLM (RBS 2 h), µg/cm²	Cast (RBS 168 h), µg/cm²	SLM (RBS 168 h), µg/cm²
Co	0.46	0.20	1.5	0.47
Cr	0.036	0.029	0.089	0.048
Mo	0.019	0.004	0.052	0.007

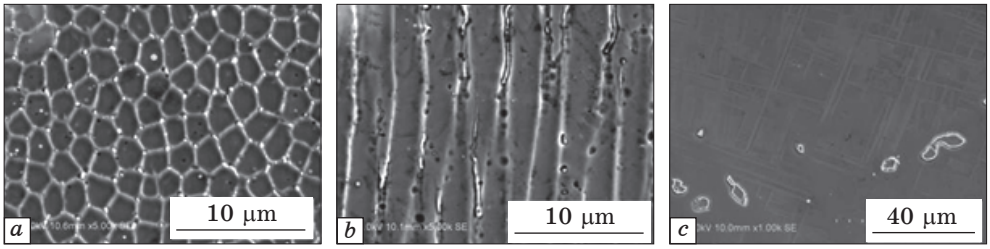

Fig. 11. Microstructures of the SLM builds and as-cast samples: (*a*) OM image of 200 W to 0.1 mm taken from the transverse cross-section normal to the printing direction; (*b*) OM image of 200 W to 0.1 mm taken from the vertical cross-section parallel to the printing direction; (*c*) OM image of the as-cast alloy [58]

compared with 2 h. The SLM alloy samples generally released less Co, Mo, and total amounts of metal ions than the cast samples. It can be concluded that the total metal ion release increased in the following order for the SLM and cast samples: R40 ≈ L20 < R20 < cast. The rapid cooling and strong temperature gradient during the laser melting process induced the formation of the fine cellular microstructure with the Mo-enriched cell boundaries, and the formation of large micron-sized carbides and martensitic ε-phase is suppressed. The unique texture formed by the melt pool is believed to explain observed differences between the differently fabricated laser-melted Co–Cr–Mo alloys' samples.

Amounts of Co, Cr, and Mo, released from the SLM samples with different laser power and the cast Co–29Cr–6Mo (mas.%) alloy samples in the 1% lactic acid were determined in [58]. To optimize the SLM printing parameters for the Co–29Cr–6Mo alloy samples, the laser power and scan spacing varied between 75 to 200 W and 0.1 to 0.3 mm, respectively. The laser scan speed and powder stacking thickness were fixed at 50 mm·s^{-1} and 0.05 mm, respectively. Figure 11 shows the microstructures of the SLM printed and the as-cast samples. Circular arch-shaped boundaries and fine particles were observed in the optical microscope (OM) image taken from the transverse cross-section normal to the printing direction. SEM observation revealed that the latter included cellular dendrites with a diameter of about 2.7 μm. In the transverse cross-section parallel to the printing direction, gradual arch-shaped boundaries were observed almost normal to the printing direction. The boundary spacing nearly agreed with the stacking thickness of the powders (0.05 mm). Therefore, the boundaries may correspond to the fusion boundaries, which were formed by laser scans. In addition, fine lamellae elongated to the building direction were observed in the vertical cross-section. This indicates that the cellular dendrites were grown along the printing direction. Such microscopic features were different from those of the as-cast samples, which consisted of the coarse dendrites with the large particles, as shown in

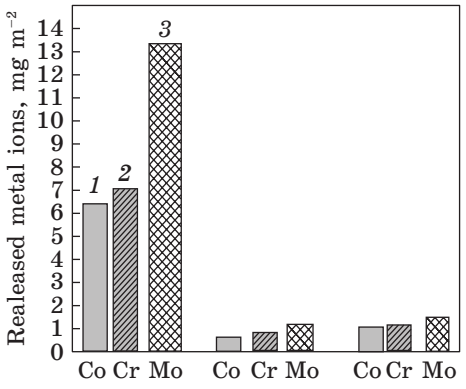

Fig. 12. Amounts of Co, Cr, and Mo, released from the SLM printing (*1*, *2*) and as-cast (*3*) samples in the 1% lactic acid after 30 days exposure: *1* — 200 W laser; *2* — 150 W laser [58]

Fig. 11. According to x-ray data, the γ phase was dominant in the SLM printed samples. The cast samples are characterized by the presence of the γ and ε phases coexisted because of the martensite transformation from the γ phase to the ε phase during fast cooling.

For metal-release experiments, the plate-shaped samples were polished with waterproof emery paper (up to 800 grits) and then ultrasonically cleaned with acetone for 10 min. The polished samples were placed in the polypropylene bottles and 20 ml of a 1 mas.% lactic acid solution was poured into each bottle. The samples were immersed in the solution at 310 K for 604.8 ks (7 days) and 2592 ks (30 days). The concentrations of Co, Cr, and Mo released into the solution were determined using inductively coupled plasma–atomic emission spectroscopy. The amounts of Co, Cr, and Mo released from the SLM printed and as-cast alloy samples are shown in Fig. 12. For both the printed and as-cast alloy samples, the amount of released Co was higher than that of Cr and Mo. However, the amount of Co released from the printed was two times lower than that from the as-cast alloy. It was reported that the surface oxide film of the Co–Cr alloy consisted of the Co and Cr oxides [60]. When both alloy samples were immersed in 1% lactic acid, Co dissolved from the film, and the film composition changed into Cr oxide containing Mo oxide [60]. Therefore, the formation of the Co oxide in the film was possibly suppressed for the printed samples. The amount of the released metals could be closely related to the microstructure formed by the SLM printing.

In Ref. [61], the ion release rates of the SLM-manufactured and cast Co–Cr–Mo alloy samples were compared. The Co–Cr–Mo alloy powder containing (wt.%) Co balance, Cr 29.4, Mo 6, Si 0.8, Mn 0.75, and Fe 0.26 was used in this study with the particle size distribution 22–28 μm. The following parameters of the SLM processing were used: laser power of 170 W; the scanning speed of 500 mm/s; the scan spacing of 80 μm; and a processing thickness of 35 μm. Before the experiment, all samples were sanded with sandpaper and went through the surface polishing treatment, took the ultrasonic cleaning with ethanol and deionized water in turn for 10 min and dry in the oven at 40 °C temperature for 10 min. Ion release conditions were determined after emersion to the artificial saliva (Na_2HP_4, 0.260 g/L; NaCl, 0.700 g/L; KSCN, 0.330 g/L; KH_2PO_4, 0.200 g/L; $NaHCO_3$, 1.500 g/L; KCl, 1.200 g/L, pH = 7).

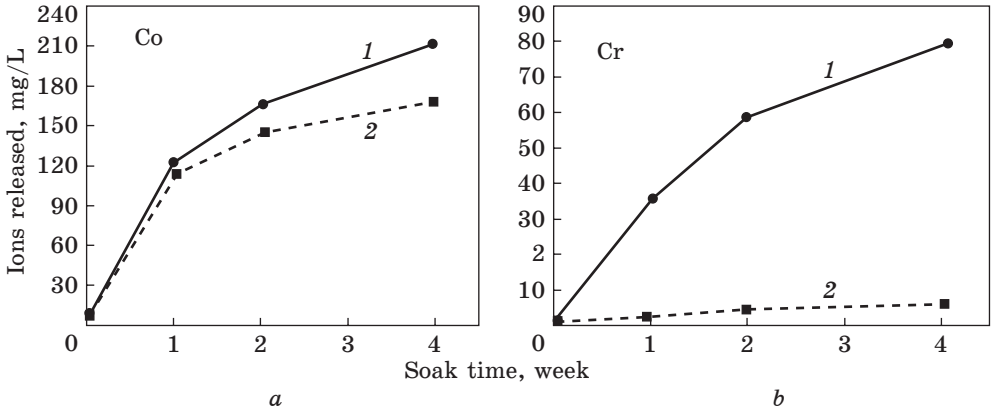

Fig. 13. Ions released from Co–Cr alloy SLM (*1*) and cast (*2*) samples during the study period in the artificial saliva, where *a* — Co release, *b* — Cr release [61]

Figure 13 indicates the concentrations of Co and Cr ions released by SLM-printed and that of the cast samples. Although Fig. 13, *a* shows that the release of Co ions at one week was almost the same for both the SLM and cast samples in artificial saliva, the release of Co ions of the cast parts was otherwise clearly larger than that of the SLM-printed samples with increasing time. Figure 4, *b* demonstrates a large difference between the quantities of Cr ions released from SLM and cast samples in the artificial saliva. One can see that the quantity of the ions did not increase with increasing time, and were lower in SLM samples than from the cast samples. Comprehensive analysis of the possible reasons for the results above is as follows: owing to the characteristics of the cast samples the insides of which are prone to shrinkage defects, as immersion time increases the large pores resulting from surface corrosion contribute to high ion release, while the SLM-printed samples have the uniform and densified surface structure, accompanied by the advantages of having smaller surface grains and fewer pores, resulting in lower ion release effects.

In the study [62], the Co–Cr–Mo–W-based alloy samples were manufactured using the SLM-printing method. The obtained material was immersed in the SBF similar to the blood plasma to mimic the real motion of body fluids against the metal implants. The Co–Cr–Mo–W alloy powder containing (wt.%) Co 59, Cr 25, Mo 3.5, W 9.5, Si 0.8, other (C, Fe, Mn, N, Si) less than 1.5 was used for SLM samples' printing. The following SLM process parameters were used: 90 W laser power, 600 mm/s laser speed, 20-μm layer thickness, and 55 μm laser spot. The printed samples were polished using the rotating polishing machine until their roughness dropped below 0.05 μm. Reagents for preparing SBF (g/L): Sodium chloride 8.035, Sodium bicarbonate 0.355, Potassium chloride 0.225, Potassium phosphate dibasic tri-hydrate 0.231, Magnesium chloride hexahy-

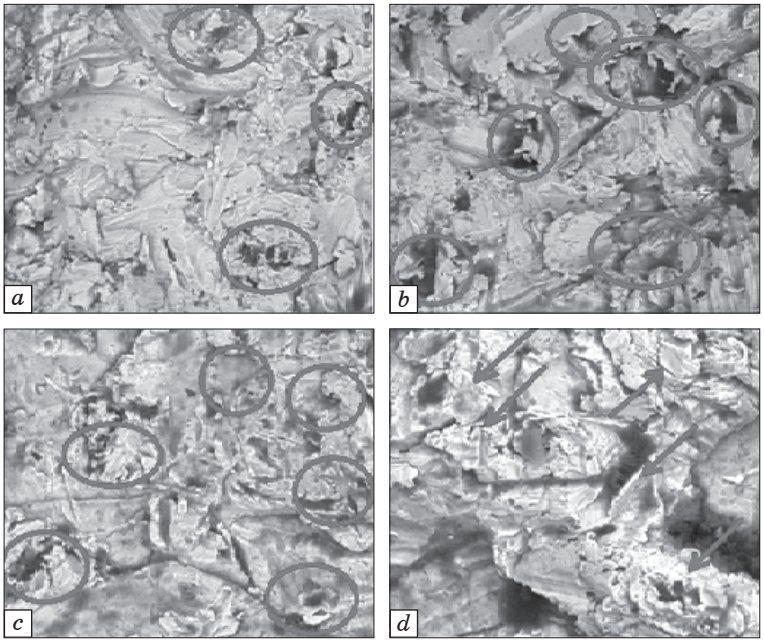

Fig. 14. SEM images showing the surface corrosion of the SLM-printed samples after SBF exposure: *a* — initial (0 h); *b* — after 15 days; *c* — after 30 days; *d* — after 60 days [62]

drate 0.311, 1M hydrochloric acid 39, Calcium chloride 0.292, Sodium sulphate 0.072, Tris (hydroxyl-methyl) amino methane 6.118 [63]. Inductively coupled plasma mass spectrometry (ICP-MS) was used to determine the concentration of the metal ions dissociated in the SBF. The surface analysis showed that during the first two weeks of exposure, the material surface was porous due to the metal ion release into the SBF and, as a direct consequence, the porous surface increased by almost 150% (Fig. 14, *b*). In the next two weeks, the formation of the oxide layer can be observed since most of the pores shrink almost 60% (Fig. 14, *c*). In the second month of exposure, the formation of the porous single crystals of Cr_2O_3 and Co_3O_4 can be observed (Fig. 14, *d*). The concentration of the Co, Cr, Mo, and Mn ions is increased, as can be observed in Table 9, where the variation of the metal ions dissociated from the samples in the SBF during the exposure period. Although the material has a large area in direct contact with SBF, a new protective layer of Co–Cr alloy is formed relatively quickly, as highlighted by the XRD data. Nevertheless, during this period, the metal ions are released in the SBF and the more concerning ones are Co and Cr. The main conclusion is that those ions form the protective oxide layer on the samples mainly due to their reactivity and lead to the passivation of the exposed surface, thus, minimizing the concentration of the ions that may dissociate into the real body fluid.

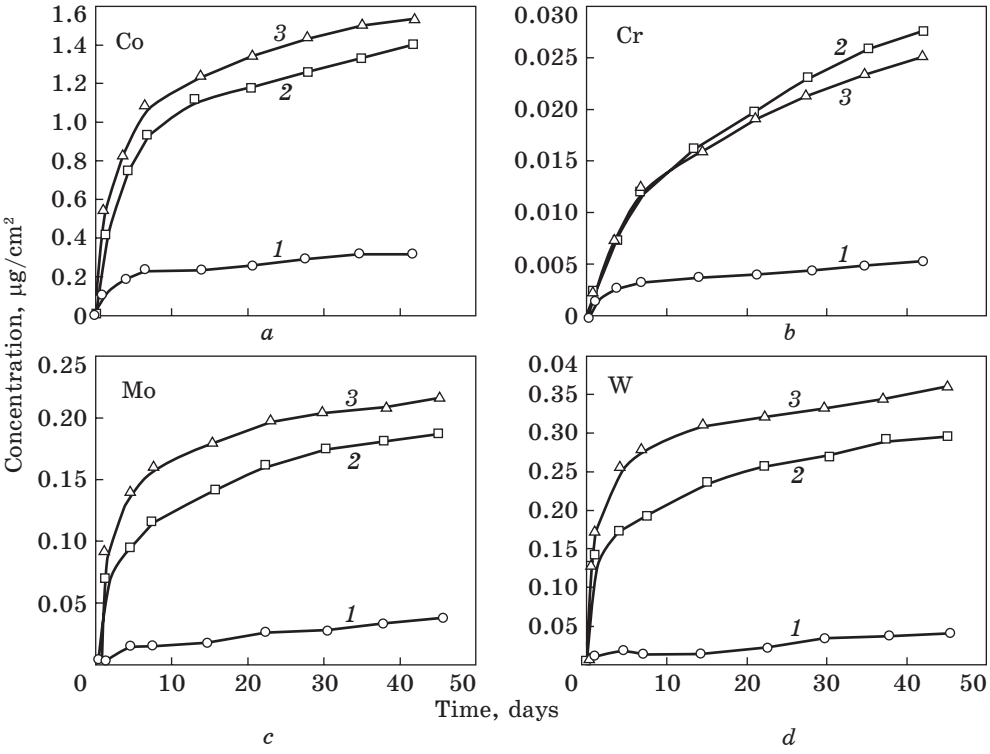

Fig. 15. Co, Cr, Mo, and W released from SLM, SLM-HT and REF Co–Cr–Mo–W alloys samples after exposure to the artificial saliva, where *1* — cast, *2* — SLM, and *3* — SLM + HT [12]

Table 9. **Measured metal ion concentrations in the SBF (μg/L) [62]**

Time, h	Co	Cr	Mo	Mn
24	5.346	7.39	0.453	0.453
72	9.771	6.852	0.729	0.729
168	14.646	6.801	1.108	1.108
336	20.32	6.58	1.611	1.611
672	30.058	6.48	2.413	2.413
1334	30.325	5.149	2.598	2.598

The ion release test of the Co–Cr–Mo–W alloy samples manufactured using different technologies, namely by SLM (as-printed and additionally post-heat-treated) and casting was investigated in Ref. [12]. The samples having the same chemical composition, containing 59% Co, 27% Cr, 9.5% W, 3.5% Mo, 1% Si, and less than 1% of C, Fe, Mn and N, were used. The first samples were SLM-printed, while the second was then additionally heat treated at 1050°C and furnace cooled (denoted as SLM-HT). SLM laser power was set at 70 W, laser travel velocity of 520 mm/s, hatch

distance of 25 μm and layer thickness of 25 μm with the calculated energy density of 215.4 J/mm^3. The third-type samples were milled from the casted prefabricated block (denoted as REF). The ion release tests were performed at the constant temperature of 37 °C in the artificial saliva (AS) with next chemical composition: 0.6 g/L NaCl, 0.72 g/L KCl, 0.22 g/L $CaCl_2 \times 2\ H_2O$, 0.68 g/L KH_2PO_4, 0.856 g/L $Na_2HPO_4 \times 12\ H_2O$, 0.060 g/L KSCN, 1.5 g/L $KHCO_3$ and 0.03 g/L citric acid (pH 6.5 ± 0.1). All samples were ground and polished until the mirrored surface was achieved, and then, electrolytically etched in 100 ml H_2O + 4 ml HCl, by applying a voltage of 5 V for 6 s, to reveal the microstructure.

The results of the ion release tests versus time exposure in AS, indicating the migration of the alloying elements (Co, Cr, Mo and W) are shown in Fig. 15. The main results are such as follow: in AS at the neutral pH, the mean release of Co ions (Fig. 15, *a*) after 42 days of exposure is higher in the SLM and SLM-HT printed samples (1.37 and 1.52 μg/mL, respectively) than in the cast samples (0.32 μg/mL). Statistical analysis showed this difference to be statistically significant, but there was no significant difference between the SLM and SLM-HT samples.

4. Conclusions

Dental metal prosthodontics is one of the most important areas of dentistry which includes fixing the dentures, veneers, bridges, crowns, implants and more that can be removable or permanently attached in the patient's mouth. In this regard, the materials of the dentures should meet the requirements of not only biocompatibility, but also good mechanical strength and corrosion resistance in intimate contact with oral tissues for the long term. It is well known that saliva and other external factors create an extremely aggressive biomechanical environment in the human oral cavity. Therefore, the corrosion resistance and chemical stability of metallic dental materials are essential for successful clinical applications. In addition, it is important to take another physiological effect into account, namely the metal ion released into the human tissue. This may have an adverse influence on the dental prosthesis performance with pain, swelling, and tissue necrosis at the site and, in some cases, its loosening. In recent years, the alloys of the Co–Cr–Mo systems have played the predominant role amongst metals used in dentistry due to their excellent mechanical properties (high hardness and ultimate strength), wear and corrosion resistance, and good biocompatibility. The literature describes the properties of such alloys with the main element composition in the following ranges (wt.%): Co 31–67, Cr 24–32, Mo 3–6, and W 8–9.

Traditionally, the lost-wax casting processes are used to produce Co–Cr-based alloys in dental prostheses. Nevertheless, using such technology it is difficult to fabricate the Co-based alloy dental components with both

high strength and complex shape. Therefore, to solve these problems, additive manufacturing is being developed as an effective way of customized dental prosthesis fabrication in dentistry. Recently, among the different AM technologies, Selective Laser Melting (SLM) has attracted the worldwide interest of research groups as a promising technique to fabricate directly the dental parts from the Co–Cr alloy system, such as dental implants, crowns, bridges and prosthetic group with complex geometry. Studies have also shown that prostheses fabricated with SLM have better corrosion resistance and higher strength than those fabricated with conventional casting methods.

The review aimed to investigate the corrosion properties and the ion release of Co–Cr alloy samples in the artificial saliva solution manufactured by different technologies, namely by SLM, additionally, heat-treated SLM and cast alloy with identical chemical compositions after exposure to artificial saline solutions. This review considers the related latest in vitro studies between 2013 and 2024. Considering the results of the reviewed studies, we can conclude as follows below.

The microstructure of the alloys was strongly influenced by the manufacturing processes. For the cast samples, the typical dendritic grains' domination and the intermetallic phases' precipitation are observed. In contrast, the SLM samples demonstrate the dendrite-like structure and cellular structure. This might indicate that these parts belonged to one solid solution, and the SLM samples had homogeneous microstructure. The grain size of the SLM samples is much smaller than that of the cast samples.

Studies have also shown that the SLM-manufactured samples have better physiological corrosion resistance as compared with those produced by conventional casting methods. The excellent corrosion resistance of the Co–Cr–Mo alloy in SBF is due to the highly protective passive (oxide) film that is the key factor for its compatibility.

According to the results of the studies and the known toxicity of Co–Cr–Mo alloys, the SLM method should be considered as the more optimal choice for the preparation of the dental parts introduced to the oral environment.

Acknowledgements. The work was partially supported by the National Academy of Sciences of Ukraine within the project 'Formation of enhanced mechanical and anti-corrosion properties of heterogeneous metallic materials by modifying atomic structure of the surface layer using intensive deformation and thermal effects' (State Reg. No. 0123U102368), grant agreement HORIZON-CL4-2023-RESILIENCE-01-33 EU-TRAINS 101130495 between the National Technical University of Ukraine 'Ihor Sikorsky Kyiv Polytechnic Institute', and the European Health and Digital Executive Agency HADEA (Towards an Ecosystem of User-centric devices and services for multisport Training and Remote healthcare enabled by an Artificial Intelligence-based Network of Sensors).

REFERENCES

1. K. Merrit, S.A. Brown, and N.A. Sharkey, *J. Biomed. Mater. Res.*, **18**: 991 (1984); https://doi.org/10.1002/jbm.820180904
2. E.N. Codaro, P. Melnikov, I. Ramires, and A.C. Guastaldi, *Russ. J. Electrochem.*, **36**: 1117 (2000); https://doi.org/10.1007/BF02757531
3. E.C. Erthridge, *Biomaterials: An Interfacial Approach* (New York: Academic Press: 1982).
4. D.F. Williams, *Biomaterials*, **29**: 2941 (2008); https://doi.org/10.1016/j.biomaterials.2008.04.023
5. B.D. Ratner, A.S. Hoffman, F.J. Schoen, and J.E. Lemons, *Biomaterials Science: an Introduction to Materials in Medicine* (New York: Academic Press: 1996).
6. C.V. Vidal and A.I. Mucoz, Electrochemical aspects in biomedical alloy characterization: Electrochemical impedance spectroscopy, *Biomedical Engineering, Trends in Materials Science* (Ed. A. Laskovski) (InTech: 2011), p. 283; https://doi.org/10.5772/13039
7. K. Prasad, O. Bazaka, M. Chua, M. Rochford, L. Fedrick, J. Spoor, R. Symes, M. Tieppo, C. Collins, A. Cao, D. Markwell, K. Ostrikov, and K. Bazaka, *Mater.*, **10**: 884 (2017); https://doi.org/10.3390/ma10080884
8. D. Rokaya, V. Srimaneepong, and J. Qin, Modification of titanium alloys for dental applications, *Metal, Metal Oxides and Metal Sulphides for Biomedical Applications. Environmental Chemistry for a Sustainable World* (Eds. S. Rajendran, M. Naushad, D. Durgalakshmi, and E. Lichtfouse) (Springer: 2021), vol. **58**, p. 51; https://doi.org/10.1007/978-3-030-56413-1_2
9. D. Rokaya, S. Bohara, V. Srimaneepong, J. Sapkota, S. Kongkiatkamon, and Z. Sultan, Metallic biomaterials for medical and dental prosthetic applications, *Functional Biomaterials* (Eds. S. Jana and S. Jana) (Springer: 2022), p. 503; https://doi.org/10.1007/978-981-16-7152-4_18
10. L.C. Lucas, R.A. Buchanan, J.E. Lemons, and C.D. Griffin, *J. Biomed. Mater. Res.*, **16**: 799 (2004); https://doi.org/10.1002/jbm.820160606
11. A. Kocijan, I. Milošec, and D.K. Merl, *J. Appl. Electrochem.*, **34**: 5 (2004); https://doi.org/10.1023/b:jach.0000021868.10122.96
12. M.B. Leban, M. Kurnik, I. Kopač, M.J. Klug, B. Podgornik, and T. Kosec, *Electrochim. Acta*, **445**: 142066 (2023); https://doi.org/10.1016/j.electacta.2023.142066
13. I. Milosev, CoCrMo alloy for biomedical applications, *Biomedical Applications Modern Aspects of Electrochemistry* (Ed. S. Djokić) (Boston, MA: Springer: 2012), vol. **55**, p 1; https://doi.org/10.1007/978-1-4614-3125-1_1
14. D.J. Blackwood, *Corrosion Reviews*, **21**: 97 (2003); https://doi.org/10.1515/corrrev.2003.21.2-3.97
15. N. Rinčič, I. Baučić, S. Miko, M. Papić, and E. Prohić, *Int. J. Collegium Antropologicum*, **27**: 99 (2003).
16. *Biomaterials Science* (Eds. B.D. Ratner, A.S. Hoffman, F.J. Schoen, and J.E. Lemons). (Elsevier: 2013).
17. F. Contu, B. Elsener, and H. Bohni, *Corrosion Sci.*, **47**: 1863 (2005); https://doi.org/10.1016/j.corsci.2004.09.003
18. A.W.E. Hodgson, S. Kurz, S. Virtanen, V. Fervel, C.A. Olsson, and S. Mischler, *Electrochim. Acta*, **49**: 2167 (2004); https://doi.org/10.1016/j.electacta.2003.12.043

19. A.I. Munoz and S. Mischler, *J. Electrochem. Soc.*, **154**: 562 (2007); https://doi.org/10.1149/1.2764238
20. C.V. Vidal and A.I. Munoz, *Corrosion Sci.*, **50**: 1954 (2008); https://doi.org/10.1016/j.corsci.2008
21. W. Elshahawy and I. Watanabe, *Tanta Dent. J.*, **11**: 150 (2014); https://doi.org/10.1016/j.tdj.2014.07.005
22. C.M. Garcia-Falcon, T. Gil-Lopez, A. Verdu-Vazquez, and J. Mirza-Rosca, *Mater. Chem. Phys.*, **260**: 124164 (2021); https://doi.org/10.1016/j.matchemphys.2020.124164
23. I. Milosev and H.H. Strehblow, *Electrochim. Acta*, **48**: 2767 (2003); https://doi.org/10.1016/S0013-4686(03)00396-7
24. A.W.E. Hodgson, S. Kurz, S. Virtanen, V. Fervel, C.-O.A. Olsson, and S. Mischler, *Electrochim. Acta*, **49**: 2167 (2004); https://doi.org/10.1016/j.electacta.2003.12.043
25. A. Mace, P. Khullar, C. Bouknight, and J.L. Gilbert, *Dent. Mater.*, **38**: 1184 (2022); https://doi.org/10.1016/j.dental.2022.06.021
26. A.L. Ramírez-Ledesma, P. Roncagliolo, M.A. Álvarez-Pérez, H.F. Lopez, and J.A. Juárez-Islas, *J. Mater. Eng. Perform.*, **29**: 1657 (2020); https://doi.org/10.1007/s11665-020-04711-2
27. H.R.A. Bidhendi and M. Pouranvari, *Metallurgical and Materials Engineering*, **17**: 13 (2011); https://doi.org/10.30544/384
28. M.C. Lucchetti, G. Fratto, F. Valeriani, E. De Vittori, S. Giampaoli, P. Papetti, V.R. Spica, and L. Manzon, *J. Prosthet. Dent.*, **114**: 602 (2015); https://doi.org/10.1016/j.prosdent.2015.03.002
29. T. Hanawa, *Mater. Sci. Eng. C*, **24**: 745 (2004); https://doi.org/10.1016/j.msec.2004.08.018
30. H. Lin and J.D Bumgardner, *Biomater.*, **25**: 1233 (2004); https://doi.org/10.1016/j.biomaterials.2003.08.016
31. Y. Okazakia and E. Gotoh, *Biomater.*, **26**: 11 (2005); https://doi.org/10.1016/j.biomaterials.2004.02.005
32. G. Can, G. Akpinar, and A. Aydin, *Eur. J. Dent.*, **1**: 86 (2007).
33. T.H. Huang, C.C. Yen, and C.T. Kao, *Am. J. Orthod. Dentofacial Orthop.*, **120**: 68 (2001); https://doi.org/10.1067/mod.2001.113794
34. P. Garhammer, G. Schmalz, K.A. Hiller, and T. Reitinger, *Clin. Oral. Investig*, **7**: (2003); https://doi.org/10.1007/s00784-003-0204-9
35. P. Garhammer, T. Reitinger, and G. Schmalz, *Clin. Oral Investig.*, **8**: 238 (2004); https://doi.org/10.1007/s00784-004-0281-4
36. M.P. Groover, *Fundamentals of Modern Manufacturing — Materials, Processes and Systems* (John Wiley and Sons: 2010).
37. H. Nesse, D. Mari Ekervik Ulstein, and M. Myhre Vaage, *J. Prosthet Dent.*, **114**: 686 (2015); https://doi.org/10.1016/j.prosdent.2015.05.007
38. M. Srivastava, S. Rathee, S. Maheshwari, and T.K. Kundra, *Additive Manufacturing: Fundamentals and Advancements* (Taylor & Francis Group: 2019).
39. D. Godec, J. Gonzalez-Gutierrez, A. Nordin, and E. Pei, *A Guide to Additive Manufacturing. Springer Tracts in Additive Manufacturing* (Springer: 2022).
40. T. Deb Roy, H.L. Wei, J.S. Zuback, T. Mukherjee, J.W. Elmer, J.O. Milewski, A.M. Beese, A. Wilson-Heid, and W. Zhang, *Prog. Mater. Sci.*, **92**: 112 (2018); https://doi.org/10.1016/j.pmatsci.2017.10.001

41. S.P. Narra, P.N. Mittwede, S.D. Wolf, and K.L. Urish, *Orthop. Clin. North. Am.*, **50**: 13 (2019); https://doi.org/10.1016/j.ocl.2018.08.009
42. M.O. Vasylyev, B.M. Mordyuk, S.M. Voloshko, and P.O. Gurin, *Prog. Phys. Met.*, **23**, No. 2: 337 (2022); https://doi.org/10.15407/ufm.23.02.337
43. M.O. Vasylyev and P.O. Gurin, *Prog. Phys. Met.*, **24**, No. 1: 106 (2023); https://doi.org/10.15407/ufm.24.01.106
44. E. Dianne Rekow, *Dental Materials*, **36**: 9 (2020); https://doi.org/10.1016/j.dental.2019.08.103
45. T. Koutsoukis, S. Zinelis, G. Eliades, K. Al-Wazzan, M.A. Rifaiy, and Y.S. Al Jabbari, *J. Prosthodont.*, **24**: 303 (2015); https://doi.org/10.1111/jopr.12268
46. K.P. Krug, A.W. Knauber, and F.P. Nothdurft, *Clin. Oral Investig.*, **19**: 401 (2015); https://doi.org/10.1007/s00784-014-1233-2
47. M. Revilla-Leyn and M. Özcan, *Curr. Oral Health Rep.*, **4**: 201 (2017); https://doi.org/10.1007/s40496-017-0152-0
48. Y.S. Hedberg, B. Quian, Z. Schen, S. Virtanen, and I.O. Wallinder, *Dent. Mater.*, **30**: 525 (2014); https://doi.org/10.1016/j.dental.2014.02.008
49. L.W. Lin, Y.F. Fang, Y.X. Liao, G. Chen, C.X. Gao, and P.Z. Zhu, *Adv. Eng. Mater.*, **21**: 1801013 (2019); https://doi.org/10.1002/adem.201801013
50. O. Alageel, B. Wazirian, B. Almufleh, and F. Tamimi, Fabrication of dental restorations using digital technologies: techniques and materials, *Digital Restorative Dentistry: A Guide to Materials, Equipment, and Clinical Procedures* (Eds. F. Tamimi and H. Hirayama) (Springer: 2019), pp. 55–91.
51. X.Z. Xin, J. Chen, N. Xiang, and B. Wie, *Cell Biochem. Biophys.*, **67**: 983 (2013); https://doi.org/10.1007/s12013-013-9593-9
52. J. Qiu, W.-Q. Yu, F.-Q. Zhang, R.J. Smales, Y.L. Zhang, and C.H. Lu, *European J. Oral Sci.*, **119**: 93 (2011); https://doi.org/10.1111/j.1600-0722.2011.00791.x
53. Y.J. Lu, S.Q. Wu, Y.L. Gan, J.L. Li, C.Q. Zhao, D.X. Zhuo, and J.X. Lin, *Mater. Sci. Eng. C*, **49**: 517 (2015); https://doi.org/10.1016/j.msec.2015.01.023
54. M. Seyedi, F. Zanotto, E. Liverani, A. Fortunato, C. Monticelli, and A. Balbo, *La Metallurgia Italiana*, **3**: 49 (2018); https://sfera.unife.it/handle/11392/2386240
55. X.Z. Xin, N. Xiang, J. Chen, and B. Wei, *Mater. Let.*, **88**: 101 (2012); https://dx.doi.org/10.1016/j.matlet.2012.08.032
56. Y.S. Hedberga, B. Qianc, Z.J. Shenc, S. Virtanena, and I.O. Wallinder, *Dental Materials*, **30**: 525 (2014); https://doi.org/10.1016/j.dental.2014.02.008
57. Y. Xin, T. Hu, and P.K. Chu, *Acta Biomater.*, **7**: 1452 (2011); https://doi.org/10.1016/j.actbio.2010.12.004
58. A. Takaichi, T. Nakamoto, N. Joko, N. Nomura, Y. Tsutsumi, S. Migita, H. Doi, S. Kurosu, and A. Chiba, *J. Mech. Behav. Biomed. Mater.*, **21**: 67 (2013); https://doi.org/10.1016/j.jmbbm.2013.01.021
59. D.C. Smith, R.M. Pillar, J.B. Metson, and N.S. McIntyre, *J. Biomed. Mater. Res.*, **25**: 1069 (1991); https://doi.org/10.1002/jbm.820250903

60. T. Hanawa, S. Hiromoto, and K. Asami, *Appl. Surf. Sci.*, **183**: 68 (2001); https://doi.org/10.1016/S0169-4332(01)00551-7
61. Z. Guoqing, Y. Yongqiang, S. Changhui, F. Fan, and Z. Zimian, *J. Med. Biol. Eng.*, **38**: 76 (2018); https://doi.org/10.1007/s40846-017-0293-6
62. R. Mirea, I.M. Biris, L.C Ceatra, R. Ene, A. Paraschiv, A.T. Cucuruz, G. Sbarcea, E. Popescu, and T. Badea, *Metals*, **11**: 857 (2021); https://doi.org/10.3390/met11060857
63. M.R.C. Marques, R. Loedberg, and M. Almukainzi, *Technologies*, **18**: 15 (2011); https://doi.org/10.3390/met11060857

Received 20.09.2024
Final version 05.02.2025

М.О. Васильєв[1], *Б.М. Мордюк*[1], *С.М. Волошко*[2], *П.О. Гурин*[3]
[1]Інститут металофізики ім. Г.В. Курдюмова НАН України,
бульв. Акад. Вернадського, 36, 03142 Київ, Україна
[2] Національний технічний університет України
«Київський політехнічний інститут імені Ігоря Сікорського»,
Берестейський проспект, 37, 03056 Київ, Україна
[3] Національний університет охорони здоров'я України ім. П.Л. Шупика,
вул. Дорогожицька, 9, 04112 Київ, Україна

ФІЗІОЛОГІЧНА КОРОЗІЯ ТА ВИДІЛЕННЯ ІОНІВ У СТОМАТОЛОГІЧНИХ СПЛАВАХ Co–Cr–Mo, ВИГОТОВЛЕНИХ ЗА ДОПОМОГОЮ АДИТИВНОГО ВИРОБНИЦТВА

Метою статті є огляд тих аспектів корозійної поведінки, які є найактуальнішими для клінічного застосування стоматологічних металевих сплавів. З погляду біосумісності розглянуто два явища корозії: деградацію поверхні стоматологічних виробів і вивільнення іонів легувальних атомів під час впливу штучного фізіологічного середовища. Тоді як корозія призводить до часткової втрати міцності матеріалу, явище вивільнення іонів спричинює цитотоксичність, алергію й інші біологічні впливи на організм людини. Зазначено, що сплави системи Co–Cr широко відомі своїм біомедичним застосуванням в ортопедичній і стоматологічній сферах завдяки низькій вартості та адекватним фізико-механічним властивостям. В огляді проаналізовано мікроструктуру та електрохімічні властивості комерційних стоматологічних сплавів Co–Cr–(Mo, W), виготовлених за допомогою традиційних методів лиття та селективного лазерного плавлення. На сьогодні селективне лазерне плавлення є найперспективнішим серед нових технологій адитивного виробництва, які використовуються для виготовлення металевих виробів у стоматології.

Ключові слова: адитивне виробництво, стоматологічні сплави, мікроструктура, стоматологія, корозія, виділення іонів.